

A pilot study of the radio-continuum emission from MASH planetary nebulae

I. S. Bojičić^{1,2,*}, Q. A. Parker^{1,3}, D. J. Frew¹, A. E. Vaughan¹, M. D. Filipović², and M. L. P. Gunawardhana^{4,1}

¹ Department of Physics and Astronomy, Macquarie University, Sydney, NSW 2109, Australia

² University of Western Sydney, Locked Bag 1797, Penrith South DC, NSW 1797, Australia

³ Australian Astronomical Observatory, Epping, NSW 1710, Australia

⁴ Sydney Institute for Astronomy, School of Physics, University of Sydney, NSW 2006, Australia

Received 01 Jan 2010, accepted 01 Jan 2010

Published online later

Key words astronomical data bases: miscellaneous - planetary nebulae: general - radiation mechanisms: thermal - radio continuum: ISM

We report an Australia Telescope Compact Array (ATCA) radio-continuum observations of 26 planetary nebulae (PNe) at wavelengths of 3 and 6 cm. This sample of 26 PNe were taken from the Macquarie/AAO/Strasbourg H α PNe (MASH) catalogue and previous lists. We investigate radio detection quality including measured and derived parameters for all detected or marginally detected PNe from this combined sample. Some 11 objects from the observed sample have been successfully detected and parametrized. Except for one, all detected PNe have very low radio surface brightnesses. We use a statistical distance scale method to calculate distances and ionised masses of the detected objects. Nebulae from this sample are found to be large (>0.2 pc in diameter) and highly diluted which indicates old age. For 21 PNe from this sample we list integrated H α fluxes and interstellar extinction coefficients, either taken from the literature or derived here from the Balmer decrement and radio to H α ratio methods. Finally, our detected fraction of the MASH pilot sample is relatively low compared to the non-MASH sub-sample. We conclude that future radio surveys of the MASH sample must involve deeper observations with better uv coverage in order to increase the fraction of detected objects and improve the quality of the derived parameters.

© 2006 WILEY-VCH Verlag GmbH & Co. KGaA, Weinheim

1 Introduction

Planetary nebulae (PNe) are the manifestation of the final evolutionary stage of low and intermediate mass stars ($1-8 M_{\odot}$). For a brief period ($< 5 \times 10^4$ yr; Frew & Parker 2010) these astrophysical phenomena evolve from compact and dusty, circumstellar envelopes detached from the parent star to the final stage when the star reaches the cooling path on the HR diagram, the ionised material starts to disperse into the surrounding interstellar medium and the luminosity of the nebula drops swiftly.

A significant number (~ 1200) of newly discovered PNe have been listed in the Macquarie/AAO/Strasbourg H α PNe (MASH) PN catalogues (Miszalski et al. 2008; Parker et al. 2006) which are a direct product of the Anglo-Australian Observatory/UK Schmidt Telescope (AAO/UKST) H α survey (Parker et al. 2005). A significant fraction of MASH PNe represent the oldest stages of PN evolution, dominating the known population at the faint end of the PN luminosity function.

Based on these discoveries, a pilot observational radio study was conducted in early 2003. This study intended to obtain and explore the radio-continuum data of a relatively

small sub-set of the newly discovered PNe. With the known benefits of the radio observational data (e.g. negligible interstellar extinction at cm wavelengths, absolute calibration, and a well studied emission mechanism) the pilot study aimed to examine some elementary physical properties of these new PNe, to test observing strategies and to confirm the viability of a large-scale observing program of the large number of MASH discoveries (Bojičić et al. 2011, in preparation).

In this paper, we present the observational techniques, the radio detection quality, together with measured and derived parameters for the detected objects. We also examined the spectral energy distributions (SEDs) and the correlation between measured radio fluxes and Balmer line fluxes estimated from the SuperCOSMOS H-alpha Survey (SHS; Gaustad et al. 2001) H α images (the MASH part of the sample) or found in the literature (the previously known fraction of the sample). We also present derived distances, radii and physical properties of the detected objects.

2 Sample selection, observations and data reduction

A group of 17 MASH PNe was randomly selected for observation with the ATCA. Care was taken that no obvious

* Corresponding author: e-mail: ivan.bojicic@mq.edu.au

Table 1 Field names, positions and general properties for PNe in the observed pilot sample. The listed coordinates designate the targeted position from the Strasbourg-ESO Catalogue of Galactic Planetary Nebulae (Acker et al. 1992, A92), Kohoutek & Kùhl (2002, K02) and the MASH I catalogue (Parker et al. 2006, P06). Column (4) is an object status flag as described in Parker et al. (2006). Columns (8) and (9) gives the morphological classification and optically determined angular diameter as found in the literature. Column (10) shows detection flags at 6 cm from this project. Objects flagged with “y” are positively detected and those with “n” not detected.

Field (1)	Name (2)	PNG (3)	Stat. ^a (4)	RAJ2000 (5)	DECJ2000 (6)	Cat (7)	Morph ^b . (8)	θ (9)	det. (10)
mA02	KeWe 2	228.5-11.4	T	06 37 39.1	-18 57 24	K02	E/B?	30	n
mA12	PHR0724-2021	234.7-02.2	L	07 24 13.1	-20 21 49	P06	A	85	n
mA08	PHR0724-1757	232.6-01.0	T	07 24 43.4	-17 57 51	P06	Rs	169	n
mA10	PHR0726-2858	242.5-05.9	T	07 26 04.8	-28 58 23	P06	R	32	n
wB11	PHR0731-2439	239.3-02.7	L	07 31 59.6	-24 39 04	P06	E	19	y
mA06	PHR0732-2825	242.6-04.4	T	07 32 17.4	-28 25 18	P06	B	27	y
wB06	PHR0745-3535	250.3-05.4	T	07 45 41.1	-35 35 04	P06	Es	51	n
wB07	PHR0755-3346	249.8-02.7	L	07 55 55.5	-33 46 00	P06	Ea	100	n
wB04	PHR0758-4243	257.8-06.9	T	07 58 26.3	-42 43 53	P06	R	25	n
mA09	M 3-2	240.3-07.6	T	07 14 49.8	-27 50 23	A92	B	11	y
wB03	A 23	249.3-05.4	T	07 43 18.0	-34 45 16	A92	R	65	y
wB10	NGC 2452	243.3-01.0	T	07 47 26.3	-27 20 07	A92	A	15	y
wB12	M 3-4	241.0+02.3	T	07 55 11.4	-23 38 13	A92	-	14	n ^c
wB09	PHR0803-3331	250.4-01.3	T	08 03 12.5	-33 31 02	P06	B	64	n
wB05	KeWe 4	257.8-05.4	T	08 05 33.7	-41 56 51	K02	R?	45	n
wA08	PHR1833-2632	007.2-08.1	T	18 33 21.5	-26 32 28	P06	Rrs	28	n
wA02	PHR1835-2751	006.2-09.1	T	18 35 44.6	-27 51 21	P06	Eam	22	y
wA03	PHR1837-2827	005.9-09.8	T	18 37 54.6	-28 27 31	P06	Eas	41	n
wA07	PHR1841-2716	007.3-10.1	T	18 41 55.0	-27 16 42	P06	Eas	14	n
wA09	PHR1848-1829	016.0-07.6	T	18 48 11.3	-18 29 43	P06	Ems	19	y
wA12	PHR1849-1952	014.8-08.4	T	18 49 24.2	-19 52 14	P06	Es	18	y
wA04	PHR1852-2749	007.9-12.5	T	18 52 51.5	-27 49 05	P06	R	22	n
wA10	PHR1857-1750	017.5-09.2	T	18 57 16.8	-17 50 53	P06	Eas	11	n
wA06	Hf 2-2	005.1-08.9	T	18 32 31.0	-28 43 21	A92	-	22	y
wA05	He 2-418	004.7-11.8	T	18 44 14.6	-30 19 37	A92	E	11	y
wA11	A 51	017.6-10.2	T	19 01 01.6	-18 12 13	A92	R	59	y

^a All PNe from A92 and K02 were designated as true (T).

^b References for morphological classification of non-MASH PNe: KeWe 2 and KeWe 4: Kerber et al. (1998); M 3-2: Perinotto & Corradi (1998a); A 23 and NGC 2452: Rauch et al. (1999); A 51: Stanghellini et al. (1993); He 2-418: Ruffle et al. (2004)

^c The wB12 field is excluded from the reduction process due to the insufficient visibility data (see text).

PN mimics (Frew & Parker 2010; Frew et al. 2010) were included in the sample. The selection criterion, based on angular diameter, was weighted toward objects with $\theta_{opt} < 40''$ which is approximately the size of the sky-projected shortest baseline in the EW352 ATCA configuration at 6 cm. A group of 10 known PNe catalogued in Acker et al. (1992) and Kohoutek & Kùhl (2002) was observed along with the selected MASH sample. In order to avoid large interruptions in observation, the main selection criterion for this group was based on their angular proximity to the previously selected MASH sample.

Selected objects were observed with the ATCA on the 12th, 13th and 14th of May 2003. Fields observed on the 12th and 13th are designated in the target listings with a preceding **mA** and **wA**, respectively, and fields observed on the third day (14th) has been designated with a preceding **wB**. We present field names, positions, general properties and detection flags (see § 3) for PNe in the observed pilot sample in Table 1. Observations were conducted at 6 cm and

3 cm, using the EW352 configuration in snap-shot mode and with a moderate total integration time on each source. The primary calibrator used for the preliminary antennae calibration and for the gain calibration was always PKS 1934-638 with an adopted flux of 2.842 Jy at 6 cm and 5.829 Jy at 3 cm. The summarised observational parameters for this pilot ATCA study are presented in Table 2.

Unfortunately, for all of the observed objects, data from antennae CA01 and CA02 (the shortest baseline) have been corrupted at the beginning and at the end of the observing runs because of the shadowing effect¹. Corrupted visibilities were flagged-out prior to the calibration process. After the initial flagging process the data-lost was approximately 15-40 per cent of the total integration time in the shortest baseline and a significant part of correlations with the CA01 antenna. The wB10 field is left with only one *uv* cut in the shortest baseline visibility data, and the wB12 field with no

¹ For a full explanation of the shadowing effect refer to Subrahmanyam & Deshpande (2004).

Table 3 Radio parameters of the ATCA radio-detected PNe.

(1) Name	(2) S_{3cm} [mJy]	(3) S_{6cm} [mJy]	(4) S_{NVSS} [mJy]	(5) θ_{3cm} [arcsec]	(6) θ_{6cm} [arcsec]	(7) θ_{opt} [arcsec]
PHR0731-2439	3.5±0.4	3.2±0.4	4.0±0.7	14±3	15±3	19
PHR0732-2825	-	0.8±0.2	-	-	-	27
M 3-2	2.8±0.3	2.3±0.3	2.6±0.5	16±4	-	11
A 23	5.1±0.5	5.1±0.6	4.2±0.6	33±7	-	65
NGC 2452	47.0±4.7	52.9±5.3	56.0±1.7	15±3	13±3	15
PHR1835-2751	1.7±0.9	1.8±0.3	-	13±4	-	22
PHR1848-1829	2.3±1.3	1.8±0.2	3.0±0.6	8±3	-	19
PHR1849-1952	2.9±0.4	3.3±0.4	-	23±6	21±5	18
Hf 2-2	4.7±0.5	3.2±0.9	4.4±0.5	23±5	-	22
He 2-418	2.3±0.9	3.2±0.4	3.1±0.5	-	-	11
A 51	7.1±3.1	9.2±1.0	7.3±1.2	62±15	69±15	59

Table 2 ATCA observational parameters for pilot study.

Observing wavelength [cm]	3	6
Observing frequency [MHz]	8640	4800
Bandwidth [MHz]	128	128
ATCA configuration	EW352	EW352
Typical size of the synthesised Beam [arcsec]	50×20	100×40
Typical integration time [min]	35 (15 ^a)	35 (15 ^a)
Typical rms noise [mJy/Beam]	~ 0.2	~ 0.2
Prim. cal. flux [Jy]:		
PKS 1934-638	5.829	2.842
Sec. cal. defect:		
0646-306 (mA fields)	1%	1%
0736-332 (wA fields)	3%	1%
1933-400 (wB fields)	1%	1%

^aDay three.

shortest baseline visibility data at all and with only two uv cuts in the longer baselines. The wB10 field fortunately contained a strong and relatively compact ($\theta < 20''$) program source. We argue that the loss of large structure information should not have a crucial effect on the final result. Due to the insufficient visibility data, the wB12 field is completely excluded from further analysis. In the wB02 field strong interference in the CA01-CA02 correlation at 3 cm was noticed (unrelated to the shadowing effect). Since this interference could not be properly flagged, this part of the data set was also excluded from further processing. The program source A 23, observed in the wB02 field, has an optically determined angular size of $65''$. Thus, we anticipated that the 3 cm flux density could be underestimated due to a lack of the flagged correlations (short baseline) data.

Further processing (calibration, deconvolution and parameterisation) was performed using standard MIRIAD procedures (Sault & Killen 2008) with no attempt to employ a self-calibration due to low signal to noise ratio in the observed fields. The “dirty” images were created using the natural weighting scheme and excluding antenna 6 (at 6 km).

Detected objects were parameterised using the IMSAD task. Measured integrated flux densities are tabulated in Table 3 (columns 2 and 3). If the IMSAD task reported a

proper deconvolution the angular diameters were calculated using the Gaussian deconvolution method as described in van Hoof (2000). The derived angular diameters from 6 cm and 3 cm maps are presented in columns (5) and (6) respectively. We note that because of the small declinations and incomplete (and non uniform) uv coverage the synthesised beams have strong eccentricities ranging from 0.87 to 0.97. Therefore, we used only a minor deconvolved diameter for the calculation of angular diameters.

We expected the influence of several systematic effects to affect the accuracy of derived parameters due to the limited integration time per field, a considerable loss of the short baseline information, the strong elongation of the synthesised beam and the intrinsic low brightness of observed objects. This pilot study gave us an excellent opportunity to measure the observational limits of MASH PN detectability, the extent of uncertainties and a chance to examine the observational components which have to be improved in the following full-scale experiment.

3 Detection quality

We detected 11 of the 26 observed objects in our radio maps (25 if we exclude the wB12 field which was not fully processed). Six detected objects are associated with PNe positions from the Acker et al. (1992) and Kohoutek & Köhl (2002) catalogues and five from the MASH I catalogue, with one object from the MASH catalogue positively detected only at 6 cm. That give us a detection quality strongly in favour of known PNe with around 60% detected, against 30% of detected MASH PNe. This two-to-one detection ratio between the known and MASH samples will not change significantly even if we exclude three PNe with optical sizes significantly larger than the synthesised beam (PHR0724-2021, PHR0724-1757, and PHR0755-3346).

The only object which is detected at only one frequency (6 cm) is PHR0732-2825. The 6 cm detection is at the 5σ threshold level and it is not a surprise that no emission is visible at 3 cm. Even though possible non-thermal emission could produce such an effect, due to its distinct bipolar morphology we have no doubt that the object in question is

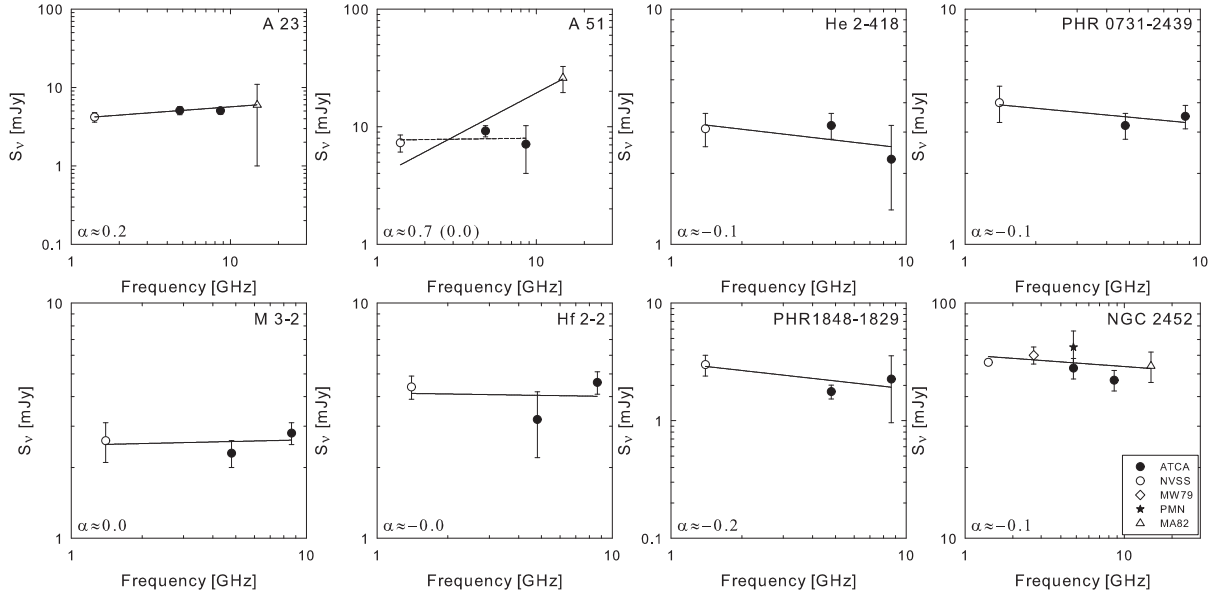


Fig. 1 The radio-continuum SED plots of PNe from the pilot sample. Filled circles represent the integrated flux densities measured from the new ATCA radio images (this paper). Other values are from: MW79 (Milne & Webster 1979); MA82 (Milne & Aller 1982); PMN (Griffith et al. 1994); NVSS (Condon et al. 1998). The straight line represent the best fit of the power-law function ($S(\nu) \propto \nu^\alpha$) to all data-points from the obtained empirical distribution. In the case of PN A 51 the power law function is also fitted to a sub-set of flux densities (ATCA and NVSS; dashed line). The value of a spectral index obtained from the best fit is given in the lower left corner.

a genuine PN and that the missing 3 cm detection is solely produced by the insufficiently sensitive observation.

Assuming that the intrinsic properties of this preliminary MASH sample conform to the general characteristics of the full MASH sample it is clear that it can be expected that most MASH PNe would be below or at the edge of sensitivity of a similar quick ATCA survey (of 1 mJy zero level noise). Obviously, faint and extended ($\theta > 100''$) PNe are not detectable using this observational configuration. Even with much larger integration times, the measured fluxes will be strongly affected by the missing flux effect.

4 Radio-continuum spectral energy distribution

With a presumption of free-free emission as the primary radio emission mechanism in PNe (Osterbrock 1989; Pottasch 1984), a construction of the SED plots can be used as a crude test of the reliability of our results.

First, a thorough literature search for published radio data of the selected sample was undertaken. We collected all radio data which can be used to cross-correlate with the obtained parameters. We found flux densities at 6 cm for M 3-2, A 23, NGC 2452 and A 51 catalogued in Cahn et al. (1992). However, the only genuine 6 cm flux density observation is for NGC 2452 (55 ± 9 mJy) originating from Milne & Aller (1975). The catalogued values for A 23 and A 51 were calculated from the 14.7 GHz flux reported in

Milne & Aller (1982) and for M 3-2 from the $H\beta$ flux from Kaler et al. (1990). We also found a 5 GHz flux density (65 ± 11 mJy) for NGC 2452 detected in the PMN Tropical survey (Griffith et al. 1994), which is in excellent agreement with the Milne & Aller (1975) value. From Milne & Aller (1982) we found flux measurements at 14.7 GHz for A 23 (6 ± 5 mJy), A 51 (26 ± 5 mJy) and NGC 2452 (54 ± 5 mJy). At 0.408 GHz we found flux upper limit of 60 ± 25 mJy (Calabretta 1982) and at 2.7 GHz we found 60 ± 10 mJy (Milne & Webster 1979) for NGC 2452. Finally, the NRAO VLA Sky Survey (NVSS: Condon et al. 1998) covers this part of the sky at 1.4 GHz. Flux densities from NVSS, for 8 detected PN, are tabulated in column (4) in Table 3. Published data, together with the data from our observations, were used for the construction of SEDs for 6 known and 2 MASH PNe (Fig. 1). All plots were produced only for objects where the independent data were available.

Except in the case of the A 51, our measurements are in a good agreement with that expected for optically thin nebulae. The spectra observed in A 51 appear to have a signature of two component emission or some additional emission mechanism at frequencies above 10 GHz. We examined this PN in more detail in section 7.

Table 4 Analysis of the extinction coefficients calculated from different methods.

Name	log F(H α)	$E(B - V)$	$E(B - V)_{6cm}$	$E(B - V)_{20cm}$
M 3-2	-12.11 ⁽¹⁾	0.56 ⁽²⁾	0.43	0.43
He 2-418	-12.05 ⁽³⁾	0.42 ⁽¹⁾	0.52	0.45
Hf 2-2	-11.63 ⁽⁴⁾	0.50 ⁽⁵⁾	0.10	0.18
A 51	-11.35 ⁽⁴⁾	0.12 ⁽⁶⁾ (0.22) ⁽⁷⁾	0.27	0.12
A 23	-11.88 ⁽⁴⁾	1.69 ⁽³⁾ (0.65) ⁽⁷⁾	0.55	0.42
KeWe 4	-12.92 ⁽⁸⁾	0.70 ⁽⁸⁾	-	-
NGC 2452	-10.81 ⁽¹⁾	0.36 ⁽⁹⁾	0.56	0.53
Name	log F(H α) ⁽¹⁰⁾	$E(B - V)$ ⁽¹¹⁾	$E(B - V)_{6cm}$	$E(B - V)_{20cm}$
PHR0724-2021	-12.47	-	-	-
PHR0732-2825	-12.67	0.51	0.53	-
PHR0726-2858	-12.76	0.26	-	-
PHR1835-2751	-13.05	-	1.26	-
PHR1837-2827	-13.18	-	-	-
PHR1841-2716	-13.72	-	-	-
PHR1848-1829	-12.67	-	0.88	1.05
PHR1849-1952	-12.50	-	0.98	-
PHR1857-1750	-13.22	-	-	-
PHR0758-4243	-13.50	0.77	-	-
PHR0745-3535	-12.38	-	-	-
PHR0755-3346	-12.07	0.65	-	-
PHR0803-3331	-12.32	0.50	-	-
PHR0731-2439	-12.53	1.19	1.00	1.03

References: ⁽¹⁾Shaw & Kaler (1989); ⁽²⁾Köppen et al. (1991); ⁽³⁾Ruffe et al. (2004); ⁽⁴⁾Frew et al. (2011, in preparation); ⁽⁵⁾Acker et al. (1991); ⁽⁶⁾Kaler (1983); ⁽⁷⁾Frew (2008); ⁽⁸⁾Kerber et al. (1998); ⁽⁹⁾Peña et al. (1998); ⁽¹⁰⁾Gunawardhana et al. (2011, in preparation); ⁽¹¹⁾this work.

5 H α surface brightness and interstellar extinction

We found published H α and/or H β fluxes and extinction coefficients for seven known PNe from this sample. All but one of these (KeWe 4) have been positively detected in our total intensity radio images. For the MASH part of the sample the integrated H α fluxes were obtained from intensity calibrated SHS images. A set of integrated H α fluxes for 14 MASH PNe were taken from Gunawardhana et al. (PASA, in preparation). The integrated fluxes, not corrected for reddening, are presented in Table 4. The colour excess $E(B - V)$ is estimated for five objects from our MASH sample with available flux-calibrated spectra using the standard Balmer decrement method. The flux in the Balmer lines (H α and H β) have been fitted with Gaussians using the IRAF² task SPLOT. For PHR0755-3346 the value for $E(B - V)$ is calculated from the $c_{H\beta}$ tabulated in Frew (2008).

It is expected that radio-continuum and Balmer lines emission will be well correlated, due to the same dependence on the nebular density, except in the case of optically thick radio-continuum emission. In the range of used frequencies (1-10 GHz), and assuming canonical electron temperature ($T_e \cong 10^4$ K) and density ratios ($n(\text{He}^+)/n(\text{H}^+) = 0.11$, and $n(\text{He}^{2+})/n(\text{H}^+) = 0.013$) the $E(B - V)$ can be calculated from the measured radio flux F_ν at frequency

ν and the measured and reddening-corrected H α flux using (Pottasch 1984):

$$\left(\frac{F_\nu}{\text{mJy}} \right) = \left(\frac{F(\text{H}\alpha)}{\text{erg cm}^{-2} \text{ s}^{-1}} \right) 1.02 \times 10^{10} T_e^{0.53} \nu^{-0.1} \quad (1)$$

where the standard theoretical ratio of H α /H β =2.85 is assumed. We list the extinction coefficients found from this method in the last two columns of Table 4.

6 Distances and Ionised Masses

Further parameterisation of the ATCA detected objects requires knowledge of reliable distances. For four previously known PNe (M 3-2, A 51, A 23 and NGC 2452) distances, calculated using some of the statistical distance scale method, have been published in Cahn et al. (1992); Kerber et al. (1998); Phillips (2004).

In this study, statistical distance scale methods from Phillips (2004), Stanghellini et al. (2008) and (Frew 2008, F08) has been used to calculate distances to the observed PNe. For the F08 scale we calculated the H α surface brightness from the integrated H α fluxes corrected for reddening. Optically determined angular sizes are used throughout our calculations as they were considered more reliable. The derived distances (D_P/kpc) and radii (R_P/pc) are tabulated in Table 5.

Considering an optically thin, ionised region of gas with approximation of constant electron temperature (T_e/K), the

² IRAF is distributed by the National Optical Astronomy Observatories, which is operated by the Association of Universities for Research in Astronomy, Inc. (AURA) under cooperative agreement with the National Science Foundation

Table 5 Derived parameters.

Name	$\log(T_b)$	D_{P04} (kpc)	D_{S08} (kpc)	D_{F08} (kpc)	D_{adopt} (kpc)	R (pc)	n_e (cm^{-3})	M_{ion} (M_\odot)
PHR0726-2858	-	-	-	8.8	8.8	0.68	<40	<0.57
PHR0731-2439	-0.2	5.4	5.0	5.4	5.3	0.24	220	0.14
PHR0732-2825	-1.1	6.9	5.4	7.7	6.7	0.44	60	0.23
PHR0755-3346	-	-	-	1.9	1.9	0.46	<20	<0.09
PHR0758-4243	-	-	-	11.4	11.4	0.69	<40	<0.59
PHR0803-3331	-	-	-	4.2	4.2	0.65	<20	<0.25
PHR1835-2751	-0.6	6.0	5.2	-	5.6	0.30	130	0.16
PHR1848-1829	-0.4	6.4	5.7	-	6.1	0.28	160	0.16
PHR1849-1952	-0.1	5.5	5.2	-	5.4	0.24	240	0.14
M 3-2	0.2	7.5	7.4	8.0	7.6	0.20	350	0.13
He 2-418	0.3	6.8	7.0	8.3	7.4	0.20	420	0.14
Hf 2-2	-0.3	5.1	4.6	4.5	4.7	0.25	180	0.13
A 51	-0.7	2.4	2.1	1.9	2.1	0.30	110	0.13
A 23	-1.0	2.8	2.2	2.9	2.6	0.41	60	0.18
NGC2452	1.3	2.7	3.3	3.4	3.1	0.11	1640	0.11

electron density (n_e/cm^{-3}) and ionised mass (M_{ion}/M_\odot) can be calculated from (Gathier 1987):

$$n_e = \zeta \times S_{6cm}^{\frac{1}{2}} T_e^{\frac{1}{4}} D^{-\frac{1}{2}} \theta^{-\frac{3}{2}} \varepsilon^{-\frac{1}{2}} \times \left(\frac{1+y+3xy}{1+y+xy} \right)^{-\frac{1}{2}}, \quad (2)$$

where $\zeta = 4.96 \times 10^2$ and:

$$M_{ion} = 1.18 \times 10^{-8} n_e D^3 \theta^3 \varepsilon \frac{1+4y}{1+y+xy}, \quad (3)$$

where S_{6cm} is the 6 cm flux density (mJy), D is the distance (kpc), θ is angular diameter (arcsec) of the source, y is the He abundance, x is the fraction of He II and ε is the volume filling factor defined as the ratio of the electron density (n_e) averaged over the volume to the electron density averaged over the mass (Daub 1982). We assumed an electron temperature of 10^4 K, He/H ratio of 0.11, average filling factor of 0.35 (Boffi & Stanghellini 1994), and that half of the He atoms are doubly ionised. The distance adopted for calculation of n_e and M_{ion} is the average of all obtained values except when one of the used methods shows a clear deviation from the mean value (in which case we used an average of the similar diameters). The estimated n_e and M_{ion} are tabulated in Table 5.

We compare derived parameters with parameters for the well known Helix Nebula (NGC 7293). The Helix Nebula is one of the best studied large, nearby and low surface brightness PN with a reliable distance estimate, based on the trigonometric parallaxes method, of only 216 pc (Benedict et al. 2009). The angular radii (seen in the radio-continuum) is ~ 5 arcmin implying the radius of the strongly ionised gas of about 0.35 pc. The radio flux at 5 GHz reported in Milne & Aller (1975) of 1.292 Jy is very likely an upper limit for the real flux considering the influence of several background sources. Following the same method of Gathier (1987), and using 0.75 for the filling factor, Young et al. (1999) determined the ionised mass of the nebula to be $\sim 0.36 M_\odot$. However, Rodríguez et al. (2002) argue that the filling factor approximation of $\varepsilon = 0.75$ is

too large for the Helix and that a more realistic value for the ionised mass is $\sim 0.074 M_\odot$ (with $\varepsilon = 0.005$) given by Boffi & Stanghellini (1994). The electron density in this nebula varies from 30 to 120 cm^{-3} (Henry et al. 1999) with a mean value in the main torus of about 60 cm^{-3} (O'Dell 1998). Scaling down the flux at 5 GHz and the angular diameter of 10 arcmin to the mean value of distances to our detected objects of 5 kpc (see Table 5) will give $S_{6cm} = 2.5$ mJy and angular diameter of $\theta = 30$ arcsec. Using the same filling factor as used in our sample ($\varepsilon = 0.35$) we calculate an electron density and ionised mass of $n_e \approx 120 \text{ cm}^{-3}$ and $M_{ion} \approx 0.17 M_\odot$ respectively. Mean values for electron density, ionised mass and radius found from the detected portion of the pilot sample (excluding NGC 2452) are 200 cm^{-3} , $0.15 M_\odot$ and 0.3 pc, respectively. Clearly, the average physical properties of PNe from our pilot sample are very similar to those of the Helix Nebula.

7 Notes on individual objects

In this section, we list individual notes on observed objects for which measured, derived or previously catalogued parameters are ambiguous or in disagreement.

7.1 Hf 2-2 (PNG005.1-08.9)

Hf 2-2 is a PN with a variable, close binary central star (De Marco et al. 2008; Lutz et al. 2010). Liu et al. (2006) presented an extreme abundance discrepancy factor (ADF) of about 70 for this nebula (the typical ADF is ~ 2 for most PNe). The ADF is a quantification of the abundance discrepancy, found in PNe and HII regions, between abundances determined from optical recombination lines and those found from collisionally excited lines (Liu 2006). A possible explanation for this discrepancy could be strong temperature gradients within the nebula (Peimbert 1967), or inner, hydrogen deficient clumps embedded in the diffuse nebula (Zhang et al. 2009). The electron density determined from

the hydrogen recombination spectrum near the Balmer jump region of $n_e \approx 400 \text{ cm}^{-3}$ (Zhang et al. 2004) is a factor of two larger than our radio-continuum determined value.

7.2 A 23 (PNG249.3-05.4)

This is a moderate excitation ($EC = 5$; Rauch et al. 1999), round PN with a distinct thin shell (Acker et al. 1992). Rauch et al. (1999) measured strong [O III] lines and did not detect He II indicating that it might be only moderately optically thin. A strong divergence from the radio flux expected from the measured $H\beta$ and constructed SED for this nebula imply the possibility of mild self-absorption effects in the radio-continuum. Due to its large angular size and the small integration time (only three 5 min cuts or 15 min of total integration time) we suggest that the integrated flux, reported here, should be taken as a lower limit. Another indicator that this object is not properly sampled is that the Gaussian fitting failed at 6 cm, while the estimated angular diameter at 3 cm is twice as small as the one determined from optical observation. On the other hand, the extinction coefficient estimated from the Balmer line ratio (Rauch et al. 1999) could be overestimated due to the possible internal absorption. Also, a deviation from the optical diameter could suggest that the majority of the measured radio emission is actually produced in some smaller structure. In order to positively distinguish between possible situations high resolution and high sensitivity radio observations are needed.

7.3 NGC 2452 (PNG243.3-01.0)

A PN ionised by a faint but extremely hot ($\sim 140 \times 10^4 \text{ K}$) Wolf-Rayet central star (Peña et al. 2001). The nebula consists of high gas density knots embedded in a diffuse body. NGC 2452 is the brightest radio object in this sample and with most independent flux measurements. Our 5 GHz flux appear to be in better agreement with the predicted optically thin SED than measurements from the PMN survey. As stated above, the excluded shortest baselines at 3 cm imply that the integrated flux from this wavelength must be considered as a lower limit. The observed flat SED down to $\sim 1 \text{ GHz}$ is in contradiction to an extremely high electron density of $\sim 40 \times 10^4 \text{ cm}^{-3}$ found by Feibelman (1999) from the [Ne IV] diagnostic. On the other hand electron density determined from the [S II] doublet diagnostic ($n_e \approx 1.5 \times 10^3 \text{ cm}^{-3}$) from Peña et al. (1998) are in excellent agreement with our estimate ($1.64 \times 10^3 \text{ cm}^{-3}$).

7.4 PHR1833-2632 (PNG007.2-08.1)

This MASH PN has an optical diameter of $28''$ but our radio image shows extended structure above 2σ larger than $1'$ and a radio peak above 5σ placed $\sim 100''$ from the centroid of the nebula. In order to determine if this extended structure is real or a possible artefact from a strong source placed $\sim 10'$ from the field centre, the 6 cm contour image is compared with the 1.4 GHz NVSS total intensity map. As can be seen

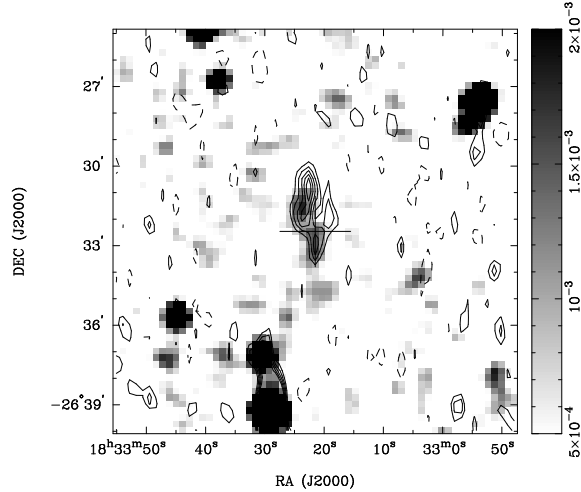


Fig. 2 NVSS total intensity map centered on the position of possible detected PN PHR1833-2632. Overlaid are contours from our 6 cm image. The contour levels are: -2, 2, 3, 4, 5 and $6 \times 0.1 \text{ mJy beam}^{-1}$. The sidebar quantifies the pixel map and its units are Jy beam^{-1} .

the extended structure in Fig. 2, which is visible in our 6 cm map, is correlated with a similar extended emission which is at the edge of the adopted zero level flux for the NVSS. This gives confidence that the observed emission is real. However, the question if this emission is actually correlated to the much smaller PN still stands open.

7.5 Abell 51 (PNG017.6-10.2)

The flux density found from a 14.7 GHz Parkes observation (Milne & Aller 1982) is almost three times larger than both the NVSS and our ATCA flux densities. The spectral energy distribution, constructed from all four measurements imply that the bulk of the radio emission, up to 14.7 GHz, is coming from an optically thick environment. However, the calculated brightness temperature at 1.4 GHz of $T_b \approx 2 \text{ K}$ and excellent agreement with the flux predicted from $H\beta$ (from Kaler (1983)) imply optically thin free-free emission at frequencies $\nu > 1 \text{ GHz}$. One can argue that both NVSS and ATCA flux measurements could be affected by the missing flux problem due to the relatively large angular size of this PN ($\theta_{\text{opt}} \approx 60''$). However, our radio determined angular diameters, at both 3 and 6 cm ($62 \pm 15''$ and $69 \pm 15''$, respectively), are in excellent agreement with the optical value which strongly imply that ATCA properly sampled this PN. Also, as stated in Condon et al. (1998), the VLA, in the used configurations, starts to be insensitive for structures larger than several arcminutes. This puts A 51 well below the NVSS filtering limit. On the other hand, the Parkes beamwidth at this frequency is $\sim 2'$. Except for a few ambiguous field detections of order of 1-2 mJy we did not find any additional and strong source in the $\sim 5'$ and $\sim 3'$ (at 6 cm and 3 cm respectively) radii from the observed PN. This allows us to conclude that the measured 14.7 GHz, if

not affected by some observational and/or systematic effect, flux should originate solely from this object. Consequently we believe that the previously published 14.7 GHz flux density of 26 mJy is greatly overestimated and that the more realistic value for the flux density at this frequency (roughly estimated from the constructed, optically thin, radio-continuum SED) is ~ 6 mJy. A deeper study of A 51 is required to resolve its intrinsic density structure.

8 Summary

Using the ATCA radio telescope a representative sample of faint and extended Galactic PNe have been observed. The sample consists of 10 previously known and 17 newly catalogued PNe from the MASH I catalogue. Some 11 objects from the observed sample have been successfully detected and parameterised. For nine partially resolved PNe we determined radio angular diameters. For six PNe these are in good agreement with optically determined values.

We examined SEDs in the cm range for eight radio-detected PNe from our sample for which we found other independent radio-continuum observations. All PNe from this sub-sample appear to emit in the radio optically thin regime which imply a more diffuse ionised medium is present.

Except for one object, all detected PNe have very low radio surface brightness. We use several statistical distance scale methods to calculate distances, electron densities and ionised masses for the detected PNe. Except for NGC 2452, all of PNe from this sample are found to be moderately large (>0.2 pc in physical diameter) and moderately to highly diluted (with electron densities in range of 60 cm^{-3} to 1640 cm^{-3} with a median of 180 cm^{-3}). The ionised masses are found to be concentrated in a relatively narrow range around $0.15 M_{\odot}$.

The results presented, together with a review of previous radio detections of MASH PNe (Bojičić et al. 2010), give us an insight into the general radio-continuum properties of this new MASH sample. From the derived physical properties we can see that detected MASH PNe are not significantly different from the known PNe sub-sample. However, it appears that, unsurprisingly, MASH PNe are placed at the faint end of the radio luminosity distribution.

The detection rate of 30% is rather poor. All future radio surveys of MASH PNe should involve significantly deeper observations with better *uv* coverage in order to improve the detection rate and quality of the derived parameters. Very careful planning of observations is necessary to reconcile limited observational time and the size of the sample which can properly represent the full catalogue. Using experience gained from this pilot study, we examined the methods and techniques which would improve our future observations. These upcoming observations will form the core of our new detailed investigation of the radio-continuum properties of MASH PNe (Bojičić et al. in preparation).

References

- Acker A., Marcout J., Ochsenbein F., Stenholm B., Tylenda R.: 1992, Strasbourg - ESO catalogue of galactic planetary nebulae. Part 1; Part 2. Garching: European Southern Observatory
- Acker A., Raytchev B., Koeppen J., Stenholm B.: 1991, A&AS, 89, 237
- Benedict, G. F., et al. 2009, AJ, 138, 1969
- Boffi F. R., Stanghellini L.: 1994, A&A, 284, 248
- Bojičić, I. S., Parker, Q. A., Filipović, M. D., & Frew, D. J. 2011, MNRAS, 412, 223
- Cahn J. H., Kaler J. B., Stanghellini L.: 1992, A&AS, 94, 399
- Calabretta M. R.: 1982, MNRAS, 199, 141
- Condon J. J., Cotton W. D., Greisen E. W., Yin Q. F., Perley R. A., Taylor G. B., Broderick J. J.: 1998, AJ, 115, 1693
- Costa R. D. D., Uchida M. M. M., Maciel W. J.: 2004, A&A, 423, 199
- Daub C. T.: 1982, ApJ, 260, 612
- De Marco O., Hillwig T. C., Smith A. J.: 2008, AJ, 136, 323
- Feibelman W. A.: 1999, ApJ, 525, 863
- Frew D. J.: 2008, PhD thesis, Macquarie University
- Frew, D. J., & Parker, Q. A. 2010, PASA, 27, 129
- Frew, D. J., Madsen, G. J., O'Toole, S. J., & Parker, Q. A.: 2010, PASA, 27, 203
- Gathier R.: 1987, A&AS, 71, 245
- Gaustad J. E., McCullough P. R., Rosing W., Van Buren D.: 2001, PASP, 113, 1326
- Griffith M. R., Wright A. E., Burke B. F., Ekers R. D.: 1994, ApJS, 90, 179
- Henry R. B. C., Kwitter K. B., Dufour R. J.: 1999, ApJ, 517, 782
- Kaler J. B.: 1983, ApJ, 271, 188
- Kaler J. B., Shaw R. A., Kwitter K. B.: 1990, ApJ, 359, 392
- Kerber F., Roth M., Manchado A., Groebner H.: 1998, A&AS, 130, 501
- Kohoutek L., Kühl D.: 2002, AN, 323, 484
- Köppen J., Acker A., Stenholm B.: 1991, A&A, 248, 197
- Liu, X.-W. 2006, Planetary Nebulae in our Galaxy and Beyond, 234, 219
- Liu X.-W., Barlow M. J., Zhang Y., Bastin R. J., Storey P. J.: 2006, MNRAS, 368, 1959
- Lutz, J., Fraser, O., McKeever, J., & Tugaga, D.: 2010, PASP, 122, 524
- Milne D. K., Aller L. H.: 1975, A&A, 38, 183
- Milne D. K., Aller L. H.: 1982, A&AS, 50, 209
- Milne D. K., Webster B. L.: 1979, A&AS, 36, 169
- Miszalski B., Parker Q. A., Acker A., Birkby J. L., Frew D. J., Kovacevic A.: 2008, MNRAS, 384, 525
- O'Dell C. R.: 1998, AJ, 116, 1346
- Osterbrock, D. E. 1989, Research supported by the University of California, John Simon Guggenheim Memorial Foundation, University of Minnesota, et al. Mill Valley, CA, University Science Books, 1989, 422 p.,
- Parker Q. A., Acker A., Frew D. J., et al.: 2006, MNRAS, 373, 79

- Parker Q. A., Philipps S., Pierce M. J., et al.: 2005, MNRAS, 362, 689
- Peimbert M.: 1967, ApJ, 150, 825
- Peña M., Stasińska G., Esteban C., Koesterke L., Medina S., Kingsburgh R.: 1998, A&A, 337, 866
- Peña M., Stasińska G., Medina S.: 2001, A&A, 367, 983
- Perinotto M., Corradi R. L. M.: 1998a, A&A, 332, 721
- Perinotto M., Corradi R. L. M.: 1998b, A&A, 332, 721
- Phillips J. P.: 2004, MNRAS, 353, 589
- Pottasch S. R.: 1984, Planetary nebulae - A study of late stages of stellar evolution. Vol. 107 of Astrophysics and Space Science Library, D. Reidel
- Rauch T., Köppen J., Napiwotzki R., Werner K.: 1999, A&A, 347, 169
- Rodríguez L. F., Goss W. M., Williams R.: 2002, ApJ, 574, 179
- Ruffle P. M. E., Zijlstra A. A., Walsh J. R., Gray M. D., Gesicki K., Minniti D., Comeron F.: 2004, MNRAS, 353, 796
- Sault B., Killen N.: 2008, MIRIAD User Guide. Aus. Teles. Nat. Fac. (ATNF), Australia
- Shaw R. A., Kaler J. B.: 1989, ApJS, 69, 495
- Stanghellini L., Corradi R. L. M., Schwarz H. E.: 1993, A&A, 279, 521
- Stanghellini L., Shaw R. A., Villaver E.: 2008, ApJ, 689, 194
- Subrahmanyam, R., & Deshpande, A. A.: 2004, MNRAS, 349, 1365
- van Hoof P. A. M.: 2000, MNRAS, 314, 99
- Young K., Cox P., Huggins P. J., Forveille T., Bachiller R.: 1999, ApJ, 522, 387
- Zhang Y., Liu X.-W., Wesson R., Storey P. J., Liu Y., Danziger I. J., 2004, MNRAS, 351, 935
- Zhang Y., Yuan H.-B., Hua C.-T., Liu X.-W., Nakashima J., Kwok S., 2009, ApJ, 695, 488